KSHV requires eIF3d for cholesterol biosynthesis to support lytic replication

Eric S. Pringle[1], Carolyn-Ann Robinson[2], Brett A. Duguay[1], Christopher S. Hughes[3], Nicolas Crapoulet[4], Andrea L-A. Monjo[1], Alexa Wilson[1], Katrina Bouzanis[1], Andrew M. Leidal[5], Stephen M. Lewis[4, 6, 7, 8], Daniel Gaston[8, 9], James Uniacke[10], Craig McCormick[1,*]

[1]Department of Microbiology & Immunology, Dalhousie University, 5850 College Street, Halifax NS, Canada B3H 4R2

[2]Arthur JE Child Comprehensive Cancer Centre, 3395 Hospital Drive NW, Calgary AB, Canada T2N 5G2

[3]Faculty of Medicine, Dalhousie University, 5849 University Ave, Halifax NS, Canada B3H 4R2

[4]Atlantic Cancer Research Institute, 35 Providence Street, Moncton NB, Canada E1C 8X3

[5]Department of Physiology and Pharmacology, 3330 Hospital Drive NW, Calgary AB, Canada

[6]Department of Chemistry and Biochemistry, Université de Moncton, Moncton NB, Canada E1A 3E9

[7]Department of Biology, University of New Brunswick, Saint John NB, Canada E2L 4L5

[8]Beatrice Hunter Cancer Research Institute, 5850 College Street, Halifax NS Canada B3H 4R2

[9]Department of Pathology, Dalhousie University, 5850 University Avenue, Halifax NS, Canada B3H 4R2

[10]Department of Molecular and Cellular Biology, University of Guelph, 50 Stone Road E., Guelph ON, Canada N1G 2W1

[*]Corresponding author: C.M., craig.mccormick@dal.ca

Running Title: eIF3d supports cholesterol biosynthesis

Keywords: KSHV; mTORC1; translation initiation; polysomes; cholesterol; translational efficiency; eIF4F; eIF3d; SQLE

ABSTRACT

Herpesvirus genomes are decoded by host RNA polymerase II, generating messenger ribonucleic acids (mRNAs) that are post-transcriptionally modified and exported to the cytoplasm. These viral mRNAs have 5′-m^{7}GTP caps and poly-adenylate (polyA) tails that should permit assembly of canonical eukaryotic initiation factor 4F (eIF4F) cap-binding complexes to initiate protein synthesis. However, we have shown that chemical disruption of eIF4F does not impede KSHV lytic replication, suggesting that alternative translation initiation factors (TIFs) support viral protein synthesis. Here we show that eIF4F and an alternative TIF known as eIF3d both contribute to the accumulation of viral proteins during KSHV lytic replication, with eIF3d supporting accumulation of viral proteins when eIF4F is depleted and *vice-versa*. However, eIF3d depletion greatly diminished release of infectious virions even when eIF4F was available to compensate for lost translation initiation capacity. This viral replication failure in the absence of eIF3d correlated with diminished accumulation of many enzymes in the cholesterol biosynthetic pathway and reduced accumulation of intracellular cholesterol. Moreover, we demonstrated that eIF3d was required to support efficient translation of essential cholesterol biosynthesis enzymes SQLE and MVK during lytic replication. These findings position eIF3d as a critical TIF not only required to support efficient translation of KSHV lytic mRNAs during times of need, but also to support the accumulation of intracellular cholesterol required to successfully complete an infectious cycle.

53 **INTRODUCTION**

54 All viruses use host translation machinery to create viral proteins. DNA viruses, such as
55 herpesviruses, replicate in the nucleus where they can access the full complement of host
56 transcription machinery [1–3]. Thus, herpesvirus mRNAs are transcribed by RNA polymerase II (Pol
57 II) and processed by enzymes that add 5′ m^7GTP caps and 3' poly-adenylate (polyA) tails, features
58 that promote mRNA stability and provide access to the same cap-dependent translation-initiation
59 factors (TIF) employed by cellular mRNAs [2,4]. In typical cell culture experiments (normoxia, rich
60 culture media, hard plastic substrate), approximately two-thirds of global protein synthesis requires
61 eIF4F [5], a protein complex comprising the m^7GTP cap-binding protein eIF4E1, the scaffolding
62 protein eIF4G1 (or eIF4G3), and the eIF4A RNA helicase [6–9]. After the cap is bound by eIF4E1,
63 eIF4G1/3 recruits eIF3 and the small ribosomal subunit to initiate scanning for the start codon.
64 eIF4A with its cofactors eIF4B and eIF4H reduce secondary structure in the 5′ untranslated region
65 (UTR) to facilitate this process [7,8].

66 In response to nutrients and growth signals, mechanistic target of rapamycin complex 1
67 (mTORC1) regulates translation initiation by promoting assembly of the eIF4F initiation complex.
68 When unphosphorylated, repressive 4E-BP1 proteins bind to the eIF4E cap-binding protein and
69 prevent recruitment the eIF4G1/3 scaffolding protein. mTORC1-mediated phosphorylation of 4E-
70 BP1 liberates eIF4E and enables eIF4F assembly and subsequent recruitment of the eIF3 complex
71 and the small ribosomal subunit [1,9,10]. mTORC1 inhibition causes widespread decreases in protein
72 synthesis, but transcripts bearing 5′ terminal oligopyrimidine (TOP) sequences [6] or pyrimidine-
73 rich translational element (PRTE) sequences [11] at their 5′ ends are especially sensitive to
74 mechanistic target of rapamycin complex 1 (mTORC1) inhibition. When eIF4F assembly is
75 inhibited in response to nutrient scarcity or treatment with mTORC1 inhibitors, residual translation
76 can be supported by eIF3d, a subunit of eIF3 that contains a cap-binding domain and can direct
77 cap-dependent translation [5,12–14]. The cap-binding domain of eIF3d is normally blocked by
78 phosphorylation by casein kinase 2 (CK2) in fed cells, but this phosphorylation is lost during
79 glucose starvation, indicating that access to eIF3d is metabolically regulated [13].

80 Herpesviruses from all subfamilies (alpha-, beta-, and gammaherpesviruses) have been
81 shown to activate mTORC1 during lytic replication [15–18], but paradoxically, virion production is
82 only modestly reduced by mTORC1 inhibition [17,19,20]. We and others have shown that eIF4F
83 assembles and remains sensitive to the mTORC1 active-site inhibitor Torin throughout the

84 Kaposi's sarcoma-associated herpesvirus (KSHV) lytic replication cycle [17,18,21]. These findings
85 suggested that translation of KSHV mRNAs can be supported alternative host TIFs during lytic
86 replication. Here, to better understand the determinants of KSHV protein synthesis in the context
87 of lytic replication, we used polysome profiling to measure translational efficiency (TE) of viral
88 mRNAs and proteomics to measure accumulation of viral proteins. We discovered that eIF4F and
89 eIF3d both contribute to the accumulation of viral proteins during KSHV lytic replication, with
90 eIF3d supporting accumulation of viral proteins when eIF4F is depleted and *vice-versa*. However,
91 eIF3d depletion greatly diminished release of infectious virions even when eIF4F was available to
92 compensate for lost translation initiation capacity. This viral replication failure in the absence of
93 eIF3d correlated with diminished accumulation of many enzymes in the cholesterol biosynthetic
94 pathway and reduced accumulation of intracellular cholesterol. Moreover, we demonstrated that
95 eIF3d was required to support efficient translation of essential cholesterol biosynthesis enzymes
96 SQLE and MVK during lytic replication. These findings position eIF3d as a critical TIF not only
97 required to support efficient translation of KSHV lytic mRNAs during times of need, but also to
98 support the accumulation of intracellular cholesterol required to successfully complete an
99 infectious cycle.
100

101 **RESULTS**

102 **eIF4F is dispensable for translation of KSHV lytic mRNAs**. We and others previously reported
103 that eIF4F assembles during KSHV latency and lytic replication and remains under strict
104 regulation by mTORC1 and 4E-BP1 [17,18]. Here, we used polysome profiling to measure how eIF4F
105 disruption affected translational efficiency (TE) of viral mRNAs. Physiologic mTORC1 activity
106 is regulated by amino acid abundance, but mTORC1 is readily inhibited by several drugs,
107 including the potent active site inhibitor Torin [21]. We observed that Torin treatment of uninfected
108 iSLK cells for 2 h prior to harvest caused dephosphorylation of ribosomal protein S6 and 4E-BP1
109 as expected, which was likewise evident in latently KSHV-infected iSLK.219 cells, or cells which
110 had been treated with doxycycline (dox) for 48 h to activate the lytic cycle (**Fig. 1A**). In these
111 experiments, we reactivated iSLK.219 cells with dox only; we omitted the HDAC inhibitor sodium
112 butyrate that is commonly used to promote lytic reactivation to limit potentially confounding
113 effects of epigenetic regulation of transcription by histone acetylation. Under these conditions,
114 many of the iSLK.219 cells either fail to reactivate or undergo abortive replication. Nevertheless,
115 it remains clear that mTORC1 regulation of canonical target proteins S6 and 4E-BP1 remain
116 largely intact during latent and lytic phases of KSHV replication. We observed that Torin treatment
117 of uninfected iSLK cells shifted mRNAs from efficiently translated heavy polysomes to poorly
118 translated sub-polysomal fractions (**Fig. 1B, top panel**) consistent with studies of other cell types
119 [6,19]. Latently infected iSLK.219 cells treated with Torin displayed a similar shift of mRNA into
120 sub-polysomal fractions (**Fig. 1B, middle panel**). By 48 h after reactivation from latency, the
121 heavy polysomes were depleted (**Fig. 1B, bottom panel**), likely due to host shutoff during lytic
122 replication [22] and the depletion of the media over the incubation time in cells in which KSHV
123 failed to reactivate from latency. In this population, Torin treatment further depleted the heavy
124 polysome fractions, although the effects were modest due to the pre-existing low translation
125 environment in these cells.

126 To measure the effects of mTORC1 inhibition on the TE of viral and host mRNAs during
127 the KSHV lytic cycle, we isolated RNA from polysome fractions from Torin- and vehicle-treated
128 cells at 48 h post-lytic reactivation (**Fig. 1B, bottom panel**) and processed it for RNA sequencing.
129 We assessed TE by simple division of the number of reads isolated from the polysomes compared
130 to the reads found in the total RNA fraction (# of reads polysome / # of reads total). The abundance
131 of KSHV transcripts in the total RNA fraction differed by as much as 100,000-fold, with ten-fold

132 more of the non-coding PAN RNA than the next most abundant RNA. **(Fig. 1C)** [2,23]. Despite these
133 differences, the TE of most viral mRNAs was similar to most cellular mRNAs, although
134 assessment of cellular mRNAs is complicated in this system because they are derived from a mixed
135 population of lytically-replicating cells and non-reactivated cells. Consistent with the literature,
136 we observed alterations in TE of cellular mRNAs in the presence of Torin, with populations of
137 mRNAs displaying increased or decreased TE **(Fig. 1D)**. The ΔTE of the majority of viral mRNAs
138 (~90%) was not inhibited or enhanced by a conservative Z-score of 1 (Z-score within 1 SD of the
139 mean in blue, Z-score > 1 SD of the mean in red). We analysed transcripts with a greater than 1.5-
140 fold change in TE using gene set enrichment analysis (GSEA) to determine how the translation of
141 cellular proteins is altered by eIF4F depletion during lytic replication[24] **(Fig. 1E)**. Gene sets
142 involved in translation elongation and initiation featured prominently in transcripts with reduced
143 TE, consistent with previous studies [6,11], which suggests that TOP-containing transcripts are
144 regulated by mTORC1 as expected during KSHV lytic replication. Notably, the TE of a gene set
145 of viral mRNAs was not significantly altered by Torin treatment. Together, these data suggest that
146 even though normal regulation of translation by the mTORC1/4E-BP/eIF4F axis is intact during
147 lytic replication, viral mRNAs continue to be efficiently translate when eIF4F is depleted.
148
149 **eIF3d is required for production of infectious KSHV virions.** When eIF4F assembly is
150 prevented by mTORC1 inhibitors, residual translation can be supported by eIF3d [5,12–14]. To assess
151 the importance of eIF3d in supporting KSHV lytic replication, we silenced *eIF3d* and measured
152 production of infectious virions at 96 h post reactivation, in the presence or absence of Torin. We
153 previously demonstrated that mTORC1 activity is required to support the earliest stages of lytic
154 replication, so Torin was added at 24 h post-reactivation to coincide with the transition to
155 mTORC1-independent viral replication. Torin treatment from 24 h to 96 h, only elicited a modest
156 reduction in production of infectious virions (**Fig. 2A**), as we have observed previously [17]. By
157 contrast, when *eIF3d* was silenced there was a ~4 $\log_{10}$ reduction in titer **(Fig. 2A)**, with very little
158 change in the abundance of viral mRNA **(Fig. 2B),** suggesting a defect in viral protein translation
159 even when eIF4F is available. Using the same experimental conditions (*eIF3d* silencing +/- Torin
160 treatment beginning at 24 h post-reactivation), we assessed the accumulation of viral proteins by
161 label-free proteomics, harvesting total protein at 72 h post-reactivation, a time point that coincides
162 with abundant late protein accumulation, following genome replication and preceding bulk virion

163 release [17]. We observed that Torin treatment had no effect on eIF3d abundance (**Fig 3A, green**
164 **circle**), whereas the siRNA targeting *eIF3d* potently and significantly reduced total eIF3d protein
165 (**Fig. 3B, green circle**), validating our RNA silencing approach. Both Torin treatment and *eIF3d*
166 silencing reduced the accumulation of most viral proteins at the 72 h time point (depicted in red
167 on the volcano plots; **Figs. 3A-B**). However, we noted differences in the specific proteins that were
168 down-regulated by inhibition of each translation initiation system (**Fig. 3C**), suggesting slightly
169 different effects on the translation of these mRNAs. Interestingly, combining both Torin treatment
170 and eIF3d knockdown resulted in an even greater suppression of viral protein accumulation (**Fig.**
171 **3D**). To determine the effect of *eIF3d* silencing on bulk translation and TE, we conducted
172 polysome analysis at 48 h post-reactivation; for this experiment *eIF3d* was silenced with a
173 lentivirus vectored shRNA, and compared to a non-specific lentivirus vector control (**Fig. 3E**).
174 The 48 h time point follows genome replication in the iSLK.219 cell model, and both late and
175 early mRNAs are present. In our experience, there are very few polysomes detectable at 72 h post-
176 reactivation. *eIF3d* silencing resulted in a strong decrease in polysomes and an increase in sub-
177 polysomal fractions (**Fig. 3E**). RT-qPCR analysis of sub-polysomal, light-polysome, and heavy-
178 polysome fractions did not reveal any significant differences in TE of select viral mRNAs when
179 eIF3d levels were reduced (**Fig. 3F**). Taken together, these data suggest that both eIF4F and eIF3d
180 contribute to accumulation of viral proteins during lytic replication, but eIF3d depletion has a far
181 greater effect on KSHV virion production.
182
183 ***eIF3d* silencing reduces levels of cholesterol biosynthesis enzymes.** Because eIF3d silencing
184 caused relatively modest decreases in viral protein accumulation compared to eIF4F depletion
185 (**Figs. 3A, 3B**), but dramatically decreased production of infectious virions by ~4 $\log_{10}$ IU/ml (**Fig.**
186 **2A**), we hypothesized that eIF3d might specifically be required for translation of host mRNAs that
187 are important for KSHV lytic replication. We once again turned to label-free proteomics of total
188 protein harvested from at 72 h post-reactivation from cells transfected with *eIF3d* siRNA
189 compared to control siRNA; this dataset used three-separate mass-charge windows to achieve
190 deeper proteome coverage than the experiment represented in **Fig 3B**. GSEA revealed that *eIF3d*
191 silencing down-regulated KSHV protein levels as expected (Figs. 4A, 4B), followed by several
192 gene sets linked to cholesterol regulation, including sterol regulatory element-binding protein
193 (SREBP), nuclear receptor subfamily 1 group H member 3 (NR1H3) and NR1H2 (also known as

194 Liver X Receptor α (LXRα) and LXRβ, respectively), and cholesterol biosynthesis. Interestingly
195 the up-regulated gene sets in proteomes from eIF3d-deficient cells generally resembled the most
196 down-regulated gene sets from our Torin treatment translatome, suggesting a compensatory
197 mechanism for eIF3d insufficiency involving increased capacity for canonical eIF4F translation.
198 This dataset stands in contrast to studies of eIF3d in human cytomegalovirus (HCMV) infection,
199 which featured regulation of unfolded protein responses but no effects on cholesterol regulation
200 [25]. This indicates that while eIF3d can be used to support translation of host mRNA, the availability
201 of those mRNA can vary during virus replication, likely due to differences in host responses, host
202 shutoff, and mRNA transcription. We focused on two cholesterol biosynthesis proteins that were
203 most significantly down-regulated for further analysis: squalene epoxidase (SQLE), which is the
204 second rate-limiting in cholesterol biosynthesis [26], after HMG-CoA reductase (HMGCR), the
205 target of statins; and mevalonate kinase (MVK), which acts on the products generated by HMGCR
206 **(Fig 4C)**.
207
208 **eIF3d is required for efficient translation of SQLE and MVK and is required for**
209 **accumulation of cholesterol during lytic replication.** To measure changes in cholesterol
210 biosynthesis genes during lytic replication we again used our proteomics datasets. Evaluating the
211 changes in lytic replication compared to latent cells, there is no change in overall eIF3d abundance
212 by 72 h post-reactivation, but there are large increases in SQLE and modest increases in HMGCS1,
213 and MVK (**Fig. 5A**), suggesting that KSHV lytic replication may furnish additional capacity in
214 cholesterol biosynthesis. When eIF3d is depleted in latently infected cells, we see an overall
215 decrease in the cholesterol biosynthesis gene set (**Figs. 5B, D**) but no significant change in MVK
216 or SQLE. By contrast, *eIF3d* silencing during lytic replication markedly decreased SQLE and
217 MVK levels (**Fig 5C**, same dataset as **Fig. 3B** with additional annotation). As an entire gene set,
218 we see that lytic replication features a general increase in cholesterol biosynthesis enzymes, and
219 *eIF3d* silencing depletes these proteins; more significantly, during lytic replication there is a drive
220 to increase cholesterol biosynthesis more so than during latency **(Fig 5D)**. Close inspection of raw
221 intensity values confirms that *eIF3d* silencing prevents the upregulation of SQLE and MVK that
222 accompanies lytic replication **(Fig. 5E)**. Using RNA retained from earlier polysome profiling
223 experiments **(Figs. 3E-F)**, we used RT-qPCR to demonstrate that *eIF3d* silencing reduces
224 translational efficiency of *SQLE* and *MVK*, moving these mRNAs from heavy into light polysome

225 fractions, whereas mRNAs encoding HMGCS and LDLR were relatively unaffected **(Fig. 5F)**,
226 consistent with their unchanged total protein abundance in eIF3d deficient cells. These eIF3d-
227 dependent effects on cholesterol biosynthesis enzymes affected intracellular cholesterol levels; we
228 observed that transition from latency to lytic replication caused substantial increases in total
229 intracellular cholesterol that were entirely dependent on eIF3d **(Fig 5G)**. These data suggest that
230 eIF3d is required to for translation of SQLE and MVK during lytic replication, and downstream
231 increases in total intracellular cholesterol.
232
233 **Statin treatment causes apoptosis of latently infected cells and reduces virion production.**
234 To measure the effects of cholesterol depletion on KSHV infected cells, we treated cells with
235 various concentrations of the HMGCR inhibitor cerivastatin at the time of lytic reactivation and
236 measured cell viability and virion production. We observed that latently infected cells were
237 sensitive to cerivastatin and there was a clear cytotoxic effect. By contrast, lytic cells and control
238 uninfected iSLK cells did not exhibit the same sensitivity to cerivastatin treatment **(Fig. 6A)**. This
239 latency-associated sensitivity to cerivastatin is consistent with previous reports of KSHV latent
240 gene products, namely v-FLIP and several viral microRNAs, that limit expression of key genes in
241 the cholesterol biosynthesis pathway; reactivation from latency limits the expression of these
242 cholesterol pathway antagonists. We conducted a western blot analysis to look for evidence of
243 apoptosis in cerivastatin-treated cells by caspase-3 activation, which is known to be active during
244 KSHV lytic replication **(Fig 6B)**[27]. Cleaved caspase 3 is clearly visible in lytic cell lysates and
245 increased with cerivastatin treatment. This corresponded with the accumulation of a faster
246 migrating ORF57 species corresponding to a previously reported caspase-cleavage product [28].
247 Higher doses of cerivastatin inhibited the accumulation of the KSHV late protein ORF65
248 Interestingly, in the latently infected cells, caspase activation was evident with only 50 nM
249 cerivastatin treatment, which greatly increased with at 500 nM, likely indicating apoptosis.
250 Similarly, lovastatin treatment also leads to apoptosis in latently infected primary effusion
251 lymphoma cell lines[29]. We measured virions production from these cells and found a very
252 consistent ~ 2 log reduction across a wide range of concentrations **(Fig. 6C)**. Together, these data
253 demonstrate that latent KSHV infection constrains cholesterol biosynthesis capacity, which is
254 rapidly reversed during lytic replication to mobilize resources necessary for efficient virion
255 production.

256 **DISCUSSION**

257 KSHV mRNAs broadly resemble their cellular counterparts, which should allow their
258 recruitment to ribosomes in an eIF4F-dependent manner. Torin treatment during lytic replication
259 depletes eIF4F and shifts TOP-containing mRNAs encoding ribosomal proteins and TIFs into sub-
260 polysomal fractions; eIF3d knockdown also depletes heavy polysomes. Heavily translated
261 polysome fractions contain viral mRNA, which remains when either eIF4F or eIF3d is depleted.
262 Despite little difference in the efficiency of translation of viral mRNAs in response to Torin
263 treatment **(Fig. 1D)** or *eIF3d* silencing **(Fig. 3F)**, there is decreased accumulation of viral proteins
264 (**Fig. 3**). Together, these data suggest that the viral mRNA is not specifically regulated or
265 dependent on either of these initiation systems and can possibly use either with similar efficiency,
266 but the availably of these systems is important to optimize viral protein synthesis throughout the
267 relatively slow-moving KSHV lytic cycle. The additive effects of Torin treatment and eIF3d
268 knockdown on viral protein accumulation are consistent with this model (**Fig. 3C**).

269 KSHV appears to access multiple translation initiation systems to maximize protein
270 production. KSHV encodes several proteins that enforce mTORC1 activation which supports
271 eIF4F formation [30]. Our data suggests that the virus is also activating eIF3d-dependent translation,
272 but the mechanism of this is not currently known. Glucose starvation has been shown to allow
273 access to the cap-binding pocket of eIF3d [13], and KSHV might use a similar metabolic signaling
274 pathway or exploiting another yet to be described regulatory pathway to access eIF3d. HIF2α is
275 stabilized in normoxia during lytic replication by ORF34[31]. This likely permits HIF2α to stimulate
276 formation of the $eIF4F_H$ hypoxic translation complex in normoxia during KSHV lytic replication,
277 which would make it available to support translation of viral mRNA [32]. $eIF4F_H$ and eIF4F are also
278 known to co-exist in cells under physiological oxygen tensions [33]. As we see decreased
279 accumulation of viral mRNA with eIF4F disassembly and eIF3d knockdown, it would suggest that
280 $eIF4F_H$ is not solely responsible for the translation of viral mRNA and would more likely act in
281 parallel with eIF4F and eIF3d. We think it is most likely that KSHV has evolved as a generalist
282 that makes use of any available translation initiation machinery to translate viral mRNA.

283 In contrast to the potentially generalist nature of KSHV mRNA, some cellular mRNAs are
284 tightly regulated by specific initiation systems. mTORC1 and LARP1 tightly regulate TOP
285 containing mRNA [6,11,34]. eIF3d has been shown to have specific client mRNAs, such as the well
286 characterized *c-Jun* and *Raptor* mRNAs that contain a long and structured 5′UTR which excludes

287 initiation by eIF4F but is compatible with eIF3d cap-binding [12,13]. The 5′UTRs of KSHV mRNA
288 are generally short compared to these cellular 5′UTRs and we think that feature might help their
289 access to different translation systems. We found that eIF3d was required for efficient translation
290 of SQLE and MVK mRNA during lytic replication (**Fig. 5F**). Neither SQLE or MVK mRNA was
291 identified as being a "eIF3d-specialized" mRNA when eIF4E was inhibited[12]. SQLE was detected
292 as binding eIF3d in a pulldown assay [13] during glucose starvation and chronic ER stress [35], which
293 further supports a role for eIF3d in supporting SQLE translation. SQLE and MVK are not regulated
294 translationally by eIF3d during HCMV infection[25], similar to what we observed in cells latently
295 infected with KSHV (**Fig. 5B**). This suggests that while eIF3d might be required for enhanced
296 cholesterol biosynthesis, it is not sufficient and likely requires the appropriate transcriptional
297 program.

298 It is currently unclear how cholesterol regulates KSHV lytic replication, or how cholesterol
299 is regulated during KSHV latency. Interestingly, HIV infected individuals who are also taking
300 statins have a 51% reduced risk of developing Kaposi's sarcoma [36], suggesting that cholesterol
301 dependency might be an easily targeted weakness of KSHV. Egress requires the nascent capsids
302 in the inner nucleus to pass through several membranes, including the inner and outer nuclear
303 membranes during primary envelopment and trans-Golgi network membranes during secondary
304 envelopment[37]. KSHV secondary envelopment has been shown to be inhibited by extracting
305 cholesterol from the cell with methyl-β-cyclodextrin [37]. In general, the amount of cholesterol in
306 membranes other than plasma membrane is relatively low, but these lower amounts of cholesterol
307 at internal membranes likely have important roles in membrane fluidity and lipid organisation. We
308 think it is likely that altered cholesterol biosynthesis by SQLE depletion or statin treatment effects
309 the ability of KSHV capsids to access or manipulate these membranes for egress. During latency,
310 KSHV alters host cell metabolism by stimulating the Warburg effect and *de novo* fatty acid
311 synthesis [38,39]. Inhibition of these metabolic adaptations with glycolysis or fatty acid synthesis
312 inhibitors leads to cell death [38,39]; we speculate it is plausible that cholesterol biosynthesis is also
313 dysregulated during latency. Taken together, our data suggests a model where KSHV mRNA is
314 efficiently translated by several different translation initiation complexes and the virus endeavours
315 to activate several to maximize protein production. Reactivation from latency though comes with
316 some specific challenges where cholesterol metabolism must be rapidly engaged and this requires

317 eIF3-dependent translation. In this way, KSHV is dependent on eIF3d not to translate its own
318 mRNA, but it requires eIF3d to support translation of essential host mRNA.
319

320 **METHODS**

321 **Cells.** Human embryonic kidney (HEK) 293T and 293A cells, as well as iSLK and iSLK.219 cells
322 (a kind gift from Don Ganem [40]), were cultured in Dulbecco's modified Eagle's medium (DMEM;
323 ThermoFisher, 11965118) supplemented with heat-inactivated 10% fetal bovine serum (FBS,
324 ThermoFisher, A31607-01), 2 mM L-Glutamine (ThermoFisher, 25030081), and 100 U/mL
325 penicillin and 100 µg/mL streptomycin (ThermoFisher, 15140122). All cells were maintained at
326 37°C in 5% CO_2 atmosphere. iSLK.219 cells were cultured with 10 mM puromycin
327 (ThermoFisher, A1113803) to maintain episome copy number of rKSHV.219; puromycin was
328 omitted from cells seeded for experiments. To induce lytic replication via expression of the RTA
329 transgene in iSLK.219 cells, 1 µg/mL of doxycycline (dox) (Sigma, D9891) was added to the cells.
330

331 **Chemicals**. Torin-1 [21], referred to as "Torin" here (Toronto Research Chemicals) was resuspended
332 in DMSO, which was used as a vehicle control at 0.1% (vol/vol) in all experiments. Unless
333 otherwise stated, Torin was used at a concentration of 250nM. Cerivastatin (Millipore Sigma,
334 SML0005) was resuspended in dH_2O.
335

336 **siRNA.** iSLK.219 cells were detached with 0.05% Trypsin-EDTA (ThermoFisher, 2530054),
337 resuspended in antibiotic-free medium, and transfected with siRNA targeting *eIF3d*
338 (ThermoFisher AM16708, Assay ID: 13732) or the negative control siRNA (ThermoFisher, Neg.
339 Control #2, 4390846) using Lipofectamine RNAiMAX (ThermoFisher, 13778075) in Opti-MEM
340 I (ThermoFisher, 31985070) as per the manufacturer's instructions. Transfection complexes were
341 mixed with cells in suspension and added to plates.
342

343 **shRNA gene silencing by transduction in suspension.** Lentiviruses derived from pLKO were
344 derived from transfection of 293T cells with packaging plasmids pMD2.G and psPAX2 (gifts from
345 Didier Trono; Addgene plasmids # 12259 and # 12260) using 1 mg/mL polyethylenimine MAX
346 (Polysciences #24765) in water. To transduce cells, iSLK.219 cells were detached with trypsin,
347 counted, and mixed with 1:20 dilution of lentivirus and 4 µg/mL polybrene (hexadimethrine
348 bromide, Sigma H9268) in suspension in a small volume (~2mL for each 15cm plate seeded) for
349 15 minutes, with frequent inversion to mix. Cells were then added to a 15 cm dish and medium
350 was topped up to 20 mL. shRNA sequences for *eIF3d* were selected from the RNAi Consortium

351 (TRCN0000156633); pLKO vectors were generated according to the RNAi Consortium shRNA
352 cloning protocol (https://portals.broadinstitute.org/gpp/public/resources/protocols). A non-
353 targeting shRNA sequence was used as a control in all experiments, pLKO-NS-BSD (a gift from
354 Keith Mostov; Addgene plasmid # 26655 [41]). Transduced cells were freshly generated for every
355 experiment; we could not derive iSLK.219 cells with stably knocked down *eIF3d* and found that
356 the cells would not re-adhere on passage. Similarly, we could not select cells and re-seed them at
357 densities appropriate for polysome analysis. Thus, the transduced cells were not selected with
358 blasticidin, and we instead relied on a low dilution/high MOI of lentivector to effectively transduce
359 the population and obtain a good knockdown.
360
361 **Cell viability.** Cells were seeded into 96-well tissue culture plates in 100 µL medium per well.
362 The next day, media was replaced with fresh media and cerivastatin at the indicated concentrations;
363 to measure the effects of cerivastatin on cell viability during lytic replication, this media change
364 included 1 µg/mL doxycycline. Cells were left to incubate with cerivastatin for 48 h prior to
365 addition of 10 µL of Cell Counting Kit 8 (CCK-8; ApexBio, K1018). Only the inner wells were
366 used to reduce variation from evaporation, and samples were seeded in triplicate. We chose to use
367 a colormetric assay instead of a fluorescence-based viability assay to avoid any potential
368 interference from the bright GFP and RFP expression from the iSLK.219 cells. After 1 h of
369 incubation with CCK-8, absorbance was read at 450 nm with correction at 600 nm using a
370 CLARIOstar Plus instrument (BMG Labtech). Values were imported into Prism (v10.6;
371 GraphPad) and 50% cytotoxic concentration (CC50) values were calculated by fitting a non-linear
372 curve to the data. The values from the 10, 5, and 2.5 µM cerivastatin treatments were separately
373 analysed by two-way ANOVA using Prism.
374
375 **Western blotting.** iSLK.219 cells were washed once with ice-cold PBS then lysed with 2x
376 Laemmli buffer (4% [wt/vol] sodium dodecyl sulfate (SDS), 20% [vol/vol] glycerol, 120 mM Tris-
377 HCl [pH 6.8]) directly in the well. DNA was sheared by repeated pipetting with a 21-gauge needle,
378 or by centrifugation through a QIAshredder column (QIAGEN) at 13,000xg for 1 min, prior to
379 100 mM dithiothreitol (DTT) addition and boiling at 95˚C for 5 min. Samples were stored at -20˚C
380 until analysis. Total protein concentration was determined by DC Protein Assay (Bio-Rad,
381 5000116) against a bovine serum albumin (BSA) (Bioshop, ALB001.25) standard curve and

382 measured in a 96-well plate format at 750 nm using an Eon (BioTek) microplate
383 spectrophotometer. Equal quantities of 10 μg total protein were loaded in each well of a
384 polyacrylamide gel and subjected to SDS-PAGE. Proteins were transferred to polyvinylidene
385 difluoride (PVDF) membranes using the Trans-Blot Turbo RTA Midi 0.2 μM PVDF Transfer Kit
386 (Bio-Rad, 1704273) and a Trans-Blot Turbo Transfer System (Bio-Rad). Membranes were blocked
387 with 5% BSA in Tris-buffered saline, 0.1% [vol/vol] Tween-20 (TBS-T) before probing overnight
388 at 4°C with the following antibodies at 1:1000 diluation: 4E-BP1 (New England Biolabs Canada
389 (NEB), #9644), β-actin (NEB #5125 or NEB #4970), cleaved caspase 3 (NEB #9664), Rps6 (S6;
390 NEB #2217) phosphoSer235/6-Rps6 (NEB #4858), ORF57 (Santa Cruz Biotechnologies sc-
391 135746), LANA (a kind gift of Don Ganem), ORF65 (a kind gift S.-J. Gao). Membranes were
392 washed with TBS-T and incubated with HRP-linked secondary antibodies diluted 1:3000 in 5%
393 BSA in TBS-T for 1 h at room temperature. Secondary antibodies used: anti-rabbit, HRP-linked
394 (NEB # 7074, 1:3000 dilution), and anti-mouse, HRP-linked (NEB, #7076). Immunoblots were
395 developed with Clarity ECL reagent (Bio-Rad, 170-5061) or Clarity Max ECL reagent (Bio-Rad,
396 170-5062) and imaged on a ChemiDoc MP Imaging System (Bio-Rad). Molecular weights were
397 determined using the Broad Range, Color Prestained Protein Standards (NEB, P7719S). Molecular
398 weights in kDa are indicated on the left of blot images. Images were analyzed using Image Lab
399 6.1 (Bio-Rad). Images were cropped and annotated using Affinity Designer (Serif).
400
401 **Virus titering.** iSLK.219 cells were seeded in a 96-well plate. In some experiments, these cells
402 were transfected with siRNAs as described above during the plating procedure. The following day,
403 the supernatant was replaced with fresh medium containing 1 μg/mL doxycycline to induce
404 reactivation from latency. For experiments where Torin was added, the drug was spiked in 24 h
405 after doxycycline addition (**Fig. 2A**); serial dilutions of cerivastatin were added at the time of
406 doxycycline addition (**Fig. 6C**). Cell supernatants were harvested at 96 h post-reactivation, diluted
407 1/20 and then used to infect 293A cells by spinoculation, whereby after the inoculum was added,
408 plates were centrifuged at 800 x *g* at 37°C for 90 min, then moved to an incubator before fixation
409 24 h later. Infected cells were counterstained with Hoechst 33342 (ThermoFisher, 62249) to label
410 DNA-containing nuclei and GFP+ cells were counted using an automated fluorescent microscope
411 and Cell Profiler [42] or Imaris Microscopy analysis software [Oxford Instruments]. The IU/mL was
412 determined by counting the number of uninfected cells and calculating the corresponding MOI.

413

414 **RT-qPCR.** Total RNA from cells was extracted using the RNeasy Plus Mini Kit (QIAGEN,
415 74134) following the manufacturer's protocol. Synthesis of cDNA was performed using the
416 Maxima H Minus First Strand cDNA Synthesis Kit (ThermoFisher Scientific, K1652) using
417 random hexamer primers. Quantitative PCRs were performed using 200 nM (final) primers, 1:250
418 (final) diluted cDNA, and 1X GoTaq qPCR Master Mix (Promega, A6002). Amplifications were
419 performed using a CFX Connect Real-Time PCR Detection System (Bio-Rad) and Bio-Rad CFX
420 Manager 3.1 software. Primer sequences are listed in **Table 1**. Due to common usage of polyA
421 signals, qRT-PCR primers could amplify mRNA originating from more than one viral promoter [2].
422 For simplicity, PCR products are referred to by the mRNA coding region targeted by the primers.
423

424 **Cholesterol quantification.** Cholesterol quantity was measured using the Cholesterol/Cholesterol
425 Ester-Glo assay (Promega, J3190) essentially as per the manufacturers' directions. iSLK.219 cells
426 transfected with siRNA and seeded in a 96 well plate in triplicate. The following day the medium
427 was refreshed and 1 µg/mL doxycycline was added to stimulate lytic replication. After 72 h the
428 supernatant was removed, the cells were washed twice with ice-cold PBS and then lysed in 50 µL
429 of the Cholesterol lysis solution and the cells were incubated for 30 min at 37°C. 10 µL of the lysis
430 solution was transferred to a white 96-well plate and mixed with 10 µL of cholesterol detection
431 reagent with esterase. The plate was then incubated at room temperature for 1 h and luminescence
432 was measured on a CLARIOstar Plus plate reader. To normalize the cholesterol measurements to
433 the number of cells in the plate, a DC protein assay was performed as described above.
434

435 **Polysome Isolation.** Polysomes were isolated by ultracentrifugation of cytosolic lysate through a
436 7-47% wt/vol linear sucrose gradient (20 mM Tris HCl, 300 mM NaCl, 25 mM $MgCl_2$ in DEPC-
437 treated or nuclease-free water) lysis buffer with RNase and protease inhibitors, as described in [43].
438 High salt conditions were used to isolate RNA from gradients and low salt conditions were used
439 for isolating proteins. Gradients were prepared using manufactures' settings on a Gradient Master
440 108 (Biocomp). For each gradient, ~8 x 10^6 iSLK.219 cells were used. Cells treated with 100
441 µg/mL cycloheximide (CHX, Acros Organics or Sigma cats) for 3 min prior to harvest. Cells were
442 washed with ice-cold phosphate buffered saline (PBS) and scraped in a tube containing the spent
443 media and PBS wash. The cells were pelleted by centrifugation for 5 min at 500 x *g* and washed

again with ice-cold PBS. Cell pellets were resuspended in lysis buffer (20 mM Tris HCl, 300 mM NaCl, 25 mM $MgCl_2$, with 1% v/v Triton X-100, 400 units/ml RNAseOUT (Invitrogen), 100 µg/mL CHX, and protease and phosphatase inhibitors) for 10 min on ice. Lysates were centrifuged for 10 min at 15,000 x *g*. The supernatant was overlaid on sucrose gradients. Gradients were centrifuged at 39,000 rpm for 90 min on a SW-41 rotor. The bottom of the centrifuge tube was punctured and 60% wt/vol sucrose was underlaid by syringe pump to collect 500 µL fractions from the top of the gradient with simultaneous A_{260} measurement using a UA-6 detector (Brandel, MD). Polysome sedimentation graphs were generated with Prism (v10.6; GraphPad).

RNA-Seq Analysis of Polysome Fractions. Total RNA or pooled fractions from heavy polysomes were isolated using Ribozol (Amresco cat) or Trizol (Thermo Fisher cat) using standard procedures, except the precipitant in the aqueous fraction was isolated using an RNeasy column (Qiagen, cat). mRNA was isolated from these total fractions using polyA enrichment (Dynabeads mRNA DIRECT Micro Purification Kit, Thermo Fisher cat) according to the manufacturer's protocol, then library preparation was performed with Ion Total RNA-Seq Kit v2.0 (Thermo Fisher cat). Library size, concentration, and quality was assessed using a 2200 TapeStation (Agilent). Libraries were sequenced on Proton sequencer (ThermoFisher Scientific) with a PI chip and the Ion PI Hi-Q Sequencing 200 Kit (cat) for 520 flows. Ion Torrent reads were processed using combined Human Hg19 and KSHV (Accession GQ994935) reference transcriptomes. The KSHV genome was manually re-annotated with the transcript definitions from KSHV2.0 [2] reference transcriptome and the Quasi-Mapping software Salmon [44]. Normalized counts per million (cpm) were estimated for individual transcripts using the R package limma [45]. Two biological replicates were combined as a geometric mean [46]. The transcripts were ordered by abundance and the mean, standard deviation (SD), and Z-score were calculated using a sliding window of 200 transcripts of similar abundance [46,47]. The most abundant 100 and the least abundant 100 transcripts used the mean and SD of the adjacent bin. Translational efficiency (TE) of a transcript treatment was determined by the formula TE = $\log_2$(polysome/total). The change in translational efficiency (DTE) = TE_{Torin}-TE_{DMSO}. We scored the difference in translational efficiencies by using a sliding-window to calculate a Z-score of each detected transcript compared to the surrounding 200 transcripts of similar abundance as measured by count per million (CPM). Who did this? You? CORES? Genewhiz?

475

476 **Polysome RT-qPCR.** iSLK.219 were reactivated with 1 µg/mL doxycycline for 48 h. Torin or
477 DMSO was added 2 h prior to harvest in high salt lysis buffer as described above. Select fractions
478 were mixed 1:1 with Trizol and isolated as per manufacturer's directions except that 30-60 µg of
479 GlycoBlue Co-Precipitant (Ambion cat) and 100 ng of *in vitro* transcribed luciferase DNA (NEB
480 T7 HiScribe cat) was added to the aqueous fractions during isopropanol precipitation [43]. The
481 resulting pellet was resuspended in water and reverse transcribed using Maxima H minus reverse
482 transcriptase with random primers. mRNA was normalized to luciferase spike to control for
483 recovery. The quantity of mRNA detected in each fraction was then calculated as a percentage of
484 the total detected in all fractions. The RNA recovery was controlled by subtracting the C_T of the
485 luciferase spike, which was assumed to be constant, from the target C_T. This ΔC_T value for each
486 fraction was then subtracted from the ΔC_T of the top fraction of the gradient to determine the
487 $\Delta\Delta C_T$. And transcript abundance (Q) was then calculated ($Q=2^{\Delta\Delta CT}$ ref for method?) for each fraction,
488 and all fractions were summed. The total quantity of a transcript is represented as a proportion of
489 the total amount of detected transcript as per [43].

490

491 **LC-MS/MS proteomics.** iSLK.219 were transfected with siRNA as described above and seeded
492 onto 6-well plates. For lytic samples, the following day cells were treated with 1 µg/mL
493 doxycycline; latent cells were untreated. For Torin treatment, drug or DMSO control was spiked
494 into the cells 24 h after addition of doxycycline. For all experiments the cells were washed once
495 with ice-cold PBS, scraped, pelleted at 500 x *g* for 5 min, then the washed once more in ice-cold
496 PBS. Afterwards the cell pellet was snap-frozen in liquid nitrogen and stored at -80°C until
497 processing.

498 Protein was extracted from cell pellets using 150 µL of a solution of 20 mM Tris-Cl pH
499 7.5, 150 mM KCl, 5 mM $MgCl_2$, 0.5% (v/v) NP-40, 0.5% (w/v) sodium deoxycholate, and 0.5X
500 cOmplete protease inhibitor (Sigma cat). To support degradation of DNA/RNA, 10 µL of a
501 nuclease solution (1 U/µL benzonase) was added to the solution and incubated at 24°C for 10 min.
502 After nuclease digestion, 50 µL of a solution of 600 mM Tris-Cl pH 7.5, 8% (w/v) SDS, and 10
503 mM dithiothreitol (DTT) was added to the tissue lysate and incubated at 95°C for 5 min in a heating
504 block. After cooling to 24°C, lysates were alkylated using 40 mM chloroacetamide (final
505 concentration) and subsequently quenched with DTT. Protein concentration of the resulting lysate

506 was measured using a BCA assay (ThermoFisher Scientific cat). Protein cleanup prior to digestion
507 was carried out using an adapted version of the previously described SP3 protocol [48,49].
508 Specifically, 1 µL of a mixture of Sera-Mag carboxylate SpeedBeads (CAT#45152105050250 and
509 CAT#65152105050250, prepared as 100 mg/mL stock solution in water) was added to 50 µg of
510 protein for each sample prior to 4X volumes of acetone. Mixtures were incubated on a
511 Thermomixer at 37°C for 5 min at 800 RPM prior to centrifugation at 5,000 x *g* for 5 min. After
512 spinning, the supernatant was discarded and beads rinsed using 800 µL of an 80% (v/v) ethanol
513 solution with pipetting to resuspend the beads. Mixtures were centrifuged at 5,000 x *g* for 5 min
514 and the supernatant discarded prior to the addition of 1 µg of trypsin/rLysC mix (Promega cat) in
515 100 µL of digestion solution (100 mM ammonium bicarbonate, 1 mM $CaCl_2$) and incubation at
516 37°C for 16 h in a Thermomixer with mixing at 800 RPM. After digestion, peptides were
517 centrifuged at 12,000 x *g* for 2 min and the supernatant recovered to a fresh tube containing 5 µL
518 of a 10% (v/v) solution of trifluoroacetic acid. To desalt peptides prior to mass spectrometry (MS)
519 analysis, an HPLC system (Agilent 1290 Infinity II with a DAD module) equipped with a reversed-
520 phase column (CORTECS T3 1.6µm, 2.1x50mm, Waters) was utilized. Specifically, peptides were
521 injected to a column equilibrated at 4% mobile phase B (0.1% formic acid in acetonitrile), rinsed
522 for 1.5 min at a flow rate of 1 mL/min, and subsequently eluted for 0.8 min at 80% mobile phase
523 B (mobile phase A = 0.1% formic acid in water). Desalted peptides were dried in a SpeedVac
524 centrifuge and reconstituted in 1% (v/v) formic acid in water at a concentration of 1 µg/µL based
525 on the 214nm UV signal from the HPLC desalting step.

526 Peptide samples were analyzed using a data-independent acquisition (DIA) acquisition
527 routine on an Orbitrap Fusion Lumos mass spectrometer (MS) (ThermoFisher Scientific). Samples
528 were introduced to the MS using an Dionex UltiMate liquid chromatography (LC) instrument
529 (ThermoFisher Scientific) equipped with a trapping-analytical column setup. For injection,
530 peptides were initially trapped using 95% mobile phase A (0.1% formic acid) on a 100 µm inner
531 diameter x 3 cm length column packed in-house with 1.9 µm Reprosil Pur C18 beads (Dr. Maisch,
532 r119.aq.). Gradient elution of peptides was performed using a ramp of mobile phase B (80% v/v
533 acetonitrile in 0.1% formic acid) on a 100 µm inner diameter x 25 cm length analytical column
534 packed with 1.9 µm Reprosil Pur C18 beads. For each injection, 1 µg of peptides were separated
535 with an 80 min LC linear gradient from 5% to 11% mobile phase B in 0.5 min, and to 34% B in
536 72.5 min at 400 nL/min, followed by rinsing and re-equilibration over the remaining 7 min. The

537 analytical column outlet was coupled to a 20 µm inner diameter LOTUS electrospray tip (Fossil
538 Ion Tech.). Data presented in **Fig. 3** and **Fig. 5**, was injected for 60 min using a single m/z range
539 (430-550 m/z). The data presented in **Fig.4** was derived from three individual injections (80-
540 minute acquisition time for each), with each acquisition covering analysis of a separate mass range
541 (injection 1 = 430 - 550, 2 = 550 - 690, 3 = 690 – 930 m/z). Specifically, the Orbitrap Lumos MS
542 was globally set to use a positive ion spray voltage of 2200 V, an ion transfer tube temperature of
543 275°C, a default charge state of 3, and an RF Lens setting of 45%. The complete duty cycle of the
544 acquisition method consisted of two MS1 scans and two sets of windowed MS2 scans (order MS1
545 - MS2 - MS1 - MS2). For the first, low mass range injection, the initial MS1 scan covered a mass
546 range of 425-555m/z at a resolution of 60,000 with an AGC target of $4e^5$ (100%) and a max
547 injection time set to 'Auto'. The following set of DIA MS2 scans covered a precursor range of
548 430-550 m/z with an isolation window size of 4 m/z (0 m/z overlap) for a total of 30 scan events.
549 Each scan used an HCD energy of 30% and covered a defined mass range of 200-1800 m/z at a
550 resolution of 30,000 with a normalized AGC target of 1000%, and the maximum injection time set
551 to 'Auto'. Loop control was set to 'N' with a value of 30 spectra. The next MS1 scan and following
552 DIA MS2 used the same settings as the previous with the exception that the MS2 precursor mass
553 range was set to 428-552 m/z to give a 2 m/z stagger with the previous scan windows. For the
554 second, medium mass range injection, the scan settings were the same as for the low mass injection
555 with the following changes: **1**) MS1 scan range of 545-695 m/z; 2. DIA-MS2 precursor scan ranges
556 of 550-690 m/z and 548-692 m/z; 3. Loop control number of spectra = 35. For the third, high mass
557 range injection, the scan settings were the same as the others with the following changes: 1. MS1
558 scan range of 685-935 m/z; **2**) DIA-MS2 precursor scan ranges of 690-930 m/z and 686-934 m/z;
559 **3**) DIA-MS2 isolation window of 8 m/z; **4**) Loop control number of spectra = 30. All scan data
560 were acquired in centroid mode. DIA-MS raw data were de-multiplexed using msconvert
561 (ProteoWizard, version 3.0.23304-e66e43d, peakPicking = 'vendor', demultiplex = overlap only,
562 10 ppm, SIM as spectra) and processed using DIA-NN (version 1.8.1)[50]. Specifically, a
563 representative human proteome fasta database (version 07/2024, 20,481 entries, includes non-
564 human contaminants) concatenated with a KSHV fasta database manually generated from
565 KSHV2.0[2] was provided to DIA-NN along with all of the raw data in order to perform an initial
566 spectral library generation step (default settings for library generation, --min-pr-mz 430 --max-pr-
567 mz 930 --min-pr-charge 2 --max-pr-charge 4, MBR disabled). Afterwards, a subset of raw files for

568 each mass range were searched together against this generated spectral library using DIA-NN with
569 'unrelated runs' activated to derive appropriate mass error and scan window settings. The entire set
570 of raw riles for each mass range were then searched against the spectral library using the derived
571 mass error and window settings with MBR enabled. Resulting report files were passed to the iq
572 package (Lib.Q.Value = 0.01, Lib.PG.Q.Value = 0.01, Q.Value = 0.01, PG.Q.Value = 0.05) in R
573 to generate estimates of protein abundance [51]. Differential protein expression was determined using
574 the R package DEqMS[52]. Volcano plots were then generated in Prism (v10.6; GraphPad).

575 **GSEA method.** The results from DEqMS were used to generate ranked gene lists using the "t"
576 statistic from lowest to highest. These ranked lists were analysed in GSEA 4.3.3 [24] using the
577 Reactome canonical pathways in the Human Molecular Signatures Database
578 (cp.c2.reactome.v2023.2.Hs.symbols) where we manually appended an additional "KSHV" gene
579 set of as used in our proteomic analysis. We used a 10% FDR as a cut off for the gene sets presented
580 in **Fig. 1E** and **Fig. 3B** [24]. Bubble plots were generated with ggplot2 in R.
581
582 **Statistics.** RT-qPCR, cholesterol quantification, and titering values were calculated in Excel
583 (Microsoft). Values were imported into Prism (v10.6; GraphPad) for statistical analysis and
584 graphing. *P* values are represented in the figures (*, $P < 0.05$; **, $P < 0.01$; ***, $P < 0.001$; ns,
585 nonsignificant).
586

587 **ACKNOWLEDGEMENTS**

588 We are grateful for the support of Gerard Gaspard, Facility Manager of the Dalhousie University
589 Cellular and Molecular Digital Imaging Core Facility for invaluable support in training,
590 troubleshooting, and data analysis. We are grateful to S-J Gao (University of Pittsburgh) for the
591 gift of KSHV ORF65 antiserum, and Don Ganem (University of California San Francisco) for the
592 gifts of KSHV LANA antiserum, iSLK cells, and iSLK.219 cells. We thank Janani Krishnan
593 (Dalhousie University) for technical support. This work was supported by Canadian Institutes for
594 Health Research Project Grant (PJT-173510) to C.M. The funders had no role in study design, data
595 collection, and interpretation, or the decision to submit the work for publication.
596
597

598 **Table 1. Oligonucleotide sequences**

	Primer sequences (5′-3′)	
qPCR Target	Forward	Reverse
luc	ACACCCGAGGGGGATGATAA	CCAGATCCACAACCTTCGCT
ORF59	CACCAGGCTTCTCCTCTGTG	TCGCTGACAGACACAGTCAC
K8.1	AGATACGTCTGCCTCTGGGT	AAAGTCACGTGGGAGGTCAC
ORF65	TGGCTCGCATGAATACCCTG	CTGCAGATGATCCCGCCTTT
ORF57	TCCAGTTTTGCTCCCCACTG	TTCTGCCGTATTGTAGGCGG
SOX	ACCACGGAGTCTGACGTCTA	ACGATCGAACTCTGCAGCAA
ORF17	GCCGGCGTATCACAAGGATA	GTGCTCCTTCATTGTCGGGA
SQLE	GCCTGCCTTTCATTGGCTTC	TTCCTTTTCTGCGCCTCCTG
MVK	AGCACCATCTGAATGCCCTC	GCTTGAGGAGTGTGATGCCA
HMGCS	TGTCCTTTCGTGGCTCACTC	CTGCAGTCTCCAGGTCTGTC
LDLR	CGTGCTCCTCGTCTTCCTTT	TCTGTCTCGAGGGGTAGCTG

599

600

601 **Figure legends**
602
603 **Fig 1. eIF4F disassembly does not affect translational efficiencies of viral mRNAs. (A)**
604 Western blots of whole cell lysates of uninfected iSLK, latently infected iSLK.219 and 48 h post-
605 doxycycline (Dox.) treatment (hpi?) iSLK.219 cells treated with 250 nM Torin or DMSO vehicle
606 control for 2 h prior to harvest. **(B)** Polysome profiles of uninfected, latent, or 48 hpi iSLK.219
607 treated with either Torin or DMSO for 2 h prior to harvest. **(C)** mRNA from translating ribosomes
608 (of DMSO treated cells) was sequenced and aligned to both the human and KSHV genomes. Viral
609 transcripts are depicted in blue on top of the grey background of cellular genes. **(D)** The Δ TE of
610 viral transcripts is depicted in blue or red on a grey background of cellular genes. Viral transcripts
611 beyond one SD of the mean are red, viral transcripts within on SD are depicted in blue. Vertical
612 lines represent a 1.5-fold change in transcript TE. **(E)** Gene set enrichment analysis of transcripts
613 TE < -1.5 Z or TE > 1.5 Z.
614
615 **Fig. 2 eIF3d is required for accumulation of KSHV lytic protein products. (A)** Viral titer at
616 96 h post-reactivation from iSLK.219 cells previously transfected with siRNA targeting eIF3d (si-
617 eIF3d) or a negative control siRNA (si-Neg) (n=3; means±SEM; statistical significance was
618 determined by two-way ANOVA). **(B)** RNA was harvested at 72h post-reactivation for RT-qPCR
619 using primers targeting viral gene products as indicated (n=4; means±SEM; statistical significance
620 was determined by two-way ANOVA). Abbreviations: nRTA, native RTA; ns, not significant;
621 tRTA, transgenic RTA.
622
623 **Fig. 3. eIF4F and eIF3d both contribute to protein accumulation during lytic replication. (A-**
624 **D)** iSLK.219 cells were transfected with siRNA targeting eIF3d (si-eIF3d) or a negative control
625 (si-Neg) and treated with doxycycline the following day. 24 h after doxycycline addition the cells
626 were treated with 250 nM Torin of DMSO vehicle control. At 72 hpi, total protein was harvested
627 for LC-MS/MS with data-independent acquisition (one m/z window) and label-free quantitation
628 (n=3). Viral proteins are graphed in red and eIF3d is labelled in green. **(A)** si-Neg Torin vs si-Neg
629 DMSO treatment demonstrating eIF4F-dependent translation. **(B)** si-eIF3d vs si-Neg
630 demonstrating eIF3d-dependent translation. **(C)** A comparison of proteins from **(A)** and **(B)** that
631 had a P.Value of < 0.05 in at least one of the samples. **(D)** si-eIF3d treated with Torin vs. si-Neg
632 cells with DMSO treatment for loss of eIF3d and eIF4F. **(E-F)** iSLK.219 cells were transduced
633 with lentiviruses encoding shRNA targeting eIF3d (sh-eIF3d) or a non-targeting (sh-NS) shRNA
634 control. 48 h after lytic induction, cells were harvested for polysome analysis. **(E)** Polysome profile
635 of sh-Neg and sh-eIF3d. **(F)** Total RNA was extracted pooled fractions from sub-polysomal, light
636 polysomes, or heavy polysomes were used for RT-qPCR analysis targeting the mRNAs indicated.
637 Data is presented as the total amount of mRNA detected in each fraction (total mRNA detected =
638 100%; n=3; means±SEM; statistical significance was determined by two-way ANOVA).
639
640 **Fig. 4. eIF3d is required for viral protein accumulation and cholesterol biosynthesis during**
641 **KSHV lytic replication.** iSLK.219 cells were transfected with siRNA targeting eIF3d (si-eIF3d)
642 or a negative control (si-Neg) and treated with doxycycline the following day. **(A)** Total protein
643 was harvested for LC-MS/MS with data-independent acquisition (three m/z windows) and label-
644 free quantitation (n=3). **(B)** Gene set enrichment analysis with 10% FDR. **(C)** Diagram of the
645 cholesterol biosynthetic pathway. Gene names for cholesterol biosynthesis enzymes are in blue.
646

Fig 5. eIF3d is required for efficient translation and accumulation of SQLE and MVK during KSHV lytic replication. (A-C) iSLK.219 cells were transfected with siRNA targeting eIF3d (si-eIF3d) or a negative control (si-Neg) and treated with doxycycline the following day. 24 h after doxycycline addition the cells were treated with 250 nM Torin of DMSO vehicle control. At 72 hpi, total protein was harvested for LC-MS/MS with data-independent acquisition (one m/z window) and label-free quantitation (n=3). Viral proteins are graphed in red; proteins related to cholesterol biosynthesis are in blue; eIF3d, SQLE, and MVK are labelled individually in green. **(A)** si-Neg Lytic vs. si-Neg Latent for changes associated with lytic replication. **(B)** si-eIF3d vs. si-Neg during latency for eIF3d-dependence in latently infected cells. **(C)** si-eIF3d vs. si-Neg in lytic cells in matched samples of **(A)** and **(B)**. **(D)** Cholesterol biosynthesis Gene set enrichment analysis (GSEA) for **(A-C)** **(E)** log2 transformed intensity value for eIF3d, SQLE, and MVK as measured for values represented in **(A-C)**. **(F)** Polysome analysis of cholesterol biosynthesis genes as in **Fig. 3E-F.** (total mRNA detected = 100%; n=3; means±SEM; statistical significance was determined by two-way ANOVA). **(G)** Quantification of cholesterol abundance by luciferase-based reporter assay normalized to total protein quantity (n=3±SEM; statistical significance was determined by two-way ANOVA)

Fig. 6. Cholesterol inhibits KSHV lytic replication (A) Uninfected iSLK, latently infected, or lytically replicating iSLK.219 cells treated with varying concentrations of HMGCR inhibitor cerivastatin. Viability was determined at 48 h using colourimetric CCK-8 assay (n=3-4; means±SEM; statistical significance was determined by one-way ANOVA). **(B)** Western blot of latent or lytic iSLK.219 at 48 hpi treated with cerivastatin for 48 h. Lysates were probed as indicated. **(C)** Virus titer at 96 hpi from iSLK.219 cells treated with varying concentrations of cerivastatin (n=3-4; means±SEM; statistical significance was determined by two-way ANOVA).

674 **References**

675 1. Glaunsinger, B. A. Modulation of the Translational Landscape During Herpesvirus Infection.
676 *Annual Review of Virology* **2**, 311–333 (2015).
677 2. Arias, C. *et al.* KSHV 2.0: a comprehensive annotation of the Kaposi's sarcoma-associated
678 herpesvirus genome using next-generation sequencing reveals novel genomic and functional
679 features. *PLoS Pathogens* **10**, e1003847 (2014).
680 3. Davis, Z. H., Hesser, C. R., Park, J. & Glaunsinger, B. A. Interaction between ORF24 and
681 ORF34 in the Kaposi's Sarcoma-Associated Herpesvirus Late Gene Transcription Factor
682 Complex Is Essential for Viral Late Gene Expression. *Journal of Virology* **90**, 599–604
683 (2015).
684 4. Ye, X., Zhaoid, Y. & Karijolich, J. The landscape of transcription initiation across latent and
685 lytic KSHV genomes. *PLoS Pathogens* **15**, 1–26 (2019).
686 5. Roiuk, M., Neff, M. & Teleman, A. A. eIF4E-independent translation is largely eIF3d-
687 dependent. *Nat Commun* **15**, 6692 (2024).
688 6. Thoreen, C. C. *et al.* A unifying model for mTORC1-mediated regulation of mRNA
689 translation. *Nature* **486**, 109–113 (2012).
690 7. Hinnebusch, A. G. The Scanning Mechanism of Eukaryotic Translation Initiation. *Annual*
691 *Review of Biochemistry* **83**, 779–812 (2014).
692 8. Merrick, W. C. eIF4F: A Retrospective. *Journal of Biological Chemistry* **290**, 24091–24099
693 (2015).
694 9. Jan, E., Mohr, I. & Walsh, D. A Cap-to-Tail Guide to mRNA Translation Strategies in Virus-
695 Infected Cells. *Annual Review of Virology* **3**, 283–307 (2016).

696 10. Pelletier, J. & Sonenberg, N. The Organizing Principles of Eukaryotic Ribosome
697 Recruitment. *Annual Review of Biochemistry* **88**, 307–335 (2019).
698 11. Hsieh, A. C. *et al.* The translational landscape of mTOR signalling steers cancer initiation
699 and metastasis. *Nature* **485**, 55–61 (2012).
700 12. Lee, A. S. Y., Kranzusch, P. J., Doudna, J. A. & Cate, J. H. D. eIF3d is an mRNA cap-
701 binding protein that is required for specialized translation initiation. *Nature* 1–16 (2016).
702 13. Lamper, A. M., Fleming, R. H., Ladd, K. M. & Lee, A. S. Y. A phosphorylation-regulated
703 eIF3d translation switch mediates cellular adaptation to metabolic stress. *Science* **856**, 853–
704 856 (2020).
705 14. Shin, S. *et al.* mTOR inhibition reprograms cellular proteostasis by regulating eIF3D-
706 mediated selective mRNA translation and promotes cell phenotype switching. *Cell Reports*
707 **42**, 112868 (2023).
708 15. Clippinger, A. J., Maguire, T. G. & Alwine, J. C. The Changing Role of mTOR Kinase in the
709 Maintenance of Protein Synthesis during Human Cytomegalovirus Infection. *Journal of*
710 *Virology* **85**, 3930–3939 (2011).
711 16. Walsh, D., Perez, C., Notary, J. & Mohr, I. Regulation of the Translation Initiation Factor
712 eIF4F by Multiple Mechanisms in Human Cytomegalovirus-Infected Cells. *Journal of*
713 *Virology* **79**, 8057–8064 (2005).
714 17. Pringle, E. S., Robinson, C.-A. & Mccormick, C. KSHV lytic replication interferes with
715 mTORC1 regulation of autophagy and viral protein synthesis. *Journal of Virology* **93**,
716 (2019).
717 18. Arias, C., Walsh, D., Harbell, J., Wilson, A. C. & Mohr, I. Activation of Host Translational
718 Control Pathways by a Viral Developmental Switch. *PLoS Pathogens* **5**, e1000334 (2009).

719 19. Lenarcic, E. M., Ziehr, B., De Leon, G., Mitchell, D. & Moorman, N. J. Differential Role for
720 Host Translation Factors in Host and Viral Protein Synthesis during Human
721 Cytomegalovirus Infection. *Journal of Virology* **88**, 1473–1483 (2014).
722 20. McMahon, R., Zaborowska, I. & Walsh, D. Noncytotoxic Inhibition of Viral Infection
723 through eIF4F-Independent Suppression of Translation by 4EGi-1. *Journal of Virology* **85**,
724 853–864 (2010).
725 21. Thoreen, C. C. *et al.* An ATP-competitive Mammalian Target of Rapamycin Inhibitor
726 Reveals Rapamycin-resistant Functions of mTORC1. *Journal of Biological Chemistry* **284**,
727 8023–8032 (2009).
728 22. Covarrubias, S. *et al.* Coordinated Destruction of Cellular Messages in Translation
729 Complexes by the Gammaherpesvirus Host Shutoff Factor and the Mammalian Exonuclease
730 Xrn1. *PLoS Pathogens* **7**, e1002339 (2011).
731 23. Davison, A. J. & Stow, N. D. New Genes from Old: Redeployment of dUTPase by
732 Herpesviruses. *Journal of Virology* **79**, 12880–12892 (2005).
733 24. Subramanian, A. *et al.* Gene set enrichment analysis: A knowledge-based approach for
734 interpreting genome-wide expression profiles. *Proc. Natl. Acad. Sci. U.S.A.* **102**, 15545–
735 15550 (2005).
736 25. Thompson, L., Depledge, D. P., Burgess, H. M. & Mohr, I. An eIF3d-dependent switch
737 regulates HCMV replication by remodeling the infected cell translation landscape to mimic
738 chronic ER stress. *Cell Reports* **39**, 110767 (2022).
739 26. Gill, S., Stevenson, J., Kristiana, I. & Brown, A. J. Cholesterol-Dependent Degradation of
740 Squalene Monooxygenase, a Control Point in Cholesterol Synthesis beyond HMG-CoA
741 Reductase. *Cell Metabolism* **13**, 260–273 (2011).

742 27. Tabtieng, T., Degterev, A. & Gaglia, M. M. Caspase-Dependent Suppression of Type I
743 Interferon Signaling Promotes Kaposi's Sarcoma-Associated Herpesvirus Lytic Replication.
744 *Journal of Virology* **92**, (2018).
745 28. Majerciak, V., Kruhlak, M., Dagur, P. K., McCoy J Philip, J. & Zheng, Z.-M. Caspase-7
746 Cleavage of Kaposi Sarcoma-associated Herpesvirus ORF57 Confers a Cellular Function
747 against Viral Lytic Gene Expression. *The Journal of biological chemistry* **285**, 11297–11307
748 (2010).
749 29. Santarelli, R. *et al.* Lovastatin reduces PEL cell survival by phosphorylating ERK1 /2 that
750 blocks the autophagic flux and engages a cross-talk with p53 to activate p21. *IUBMB Life*
751 **73**, 968–977 (2021).
752 30. Bhatt, A. P. & Damania, B. AKTivation of PI3K/AKT/mTOR signaling pathway by KSHV.
753 *Frontiers in immunology* **3**, 401 (2012).
754 31. Haque, M. & Kousoulas, K. G. The Kaposi's Sarcoma-Associated Herpesvirus ORF34
755 Protein Interacts and Stabilizes HIF-2 via Binding to the HIF-2 bHLH and PAS Domains.
756 32. Méndez-Solís, O. *et al.* Kaposi's sarcoma herpesvirus activates the hypoxia response to
757 usurp HIF2α-dependent translation initiation for replication and oncogenesis. *Cell Reports*
758 **37**, 110144 (2021).
759 33. Timpano, S. & Uniacke, J. Human Cells Cultured under Physiological Oxygen Utilize Two
760 Cap-binding Proteins to recruit Distinct mRNAs for Translation. *Journal of Biological*
761 *Chemistry* **291**, 10772–10782 (2016).
762 34. Lahr, R. M. *et al.* La-related protein 1 (LARP1) binds the mRNA cap, blocking eIF4F
763 assembly on TOP mRNAs. *eLife* **6**, (2017).

764 35. Mukhopadhyay, S., Amodeo, M. E. & Lee, A. S. Y. eIF3d controls the persistent integrated
765 stress response. *Molecular Cell* **83**, 3303-3313.e6 (2023).
766 36. Bedimo, R. J. *et al.* Statin exposure and risk of cancer in people with and without HIV
767 infection. *AIDS* **35**, 325–334 (2021).
768 37. Wang, X. *et al.* Mono-ubiquitylated ORF45 Mediates Association of KSHV Particles with
769 Internal Lipid Rafts for Viral Assembly and Egress. *PLoS Pathog* **11**, e1005332 (2015).
770 38. Delgado, T., Sanchez, E. L., Camarda, R. & Lagunoff, M. Global Metabolic Profiling of
771 Infection by an Oncogenic Virus: KSHV Induces and Requires Lipogenesis for Survival of
772 Latent Infection. *PLoS Pathogens* **8**, e1002866 (2012).
773 39. Delgado, T. *et al.* Induction of the Warburg effect by Kaposi's sarcoma herpesvirus is
774 required for the maintenance of latently infected endothelial cells. *Proc. Natl. Acad. Sci.*
775 *U.S.A.* **107**, 10696–10701 (2010).
776 40. Myoung, J. & Ganem, D. Generation of a doxycycline-inducible KSHV producer cell line of
777 endothelial origin: maintenance of tight latency with efficient reactivation upon induction.
778 *Journal of Virological Methods* **174**, 12–21 (2011).
779 41. Bryant, D. M. *et al.* A molecular network for de novo generation of the apical surface and
780 lumen. *Nature Cell Biology* **12**, 1035–1045 (2010).
781 42. Stirling, D. R. *et al.* CellProfiler 4: improvements in speed, utility and usability. *BMC*
782 *Bioinformatics* **22**, 433 (2021).
783 43. Pringle, E. S., Mccormick, C. & Cheng, Z. Polysome Profiling Analysis of mRNA and
784 Associated Proteins Engaged in Translation. *Current Protocols in Molecular Biology* **125**,
785 e79 (2018).

786 44. Patro, R., Duggal, G., Love, M. I., Irizarry, R. A. & Kingsford, C. Salmon provides fast and
787 bias-aware quantification of transcript expression. *Nature Methods* **14**, 417–419 (2017).
788 45. Ritchie, M. E. *et al.* limma powers differential expression analyses for RNA-sequencing and
789 microarray studies. *Nucleic Acids Research* **43**, e47–e47 (2015).
790 46. Quackenbush, J. Microarray data normalization and transformation. *Nature Genetics* **32**,
791 496–501 (2002).
792 47. Andreev, D. E. *et al.* Translation of 5' leaders is pervasive in genes resistant to eIF2
793 repression. *eLife* **4**, e03971 (2015).
794 48. Hughes, C. S. *et al.* Single-pot, solid-phase-enhanced sample preparation for proteomics
795 experiments. *Nat Protoc* **14**, 68–85 (2019).
796 49. Hughes, C. S. *et al.* Single-pot, solid-phase-enhanced sample preparation for proteomics
797 experiments. *Nat Protoc* **14**, 68–85 (2019).
798 50. Demichev, V., Messner, C. B., Vernardis, S. I., Lilley, K. S. & Ralser, M. DIA-NN: neural
799 networks and interference correction enable deep proteome coverage in high throughput. *Nat*
800 *Methods* **17**, 41–44 (2020).
801 51. Pham, T. V., Henneman, A. A. & Jimenez, C. R. *iq* : an R package to estimate relative
802 protein abundances from ion quantification in DIA-MS-based proteomics. *Bioinformatics* **36**,
803 2611–2613 (2020).
804 52. Zhu, Y. *et al.* DEqMS: A Method for Accurate Variance Estimation in Differential Protein
805 Expression Analysis. *Molecular & Cellular Proteomics* **19**, 1047–1057 (2020).
806

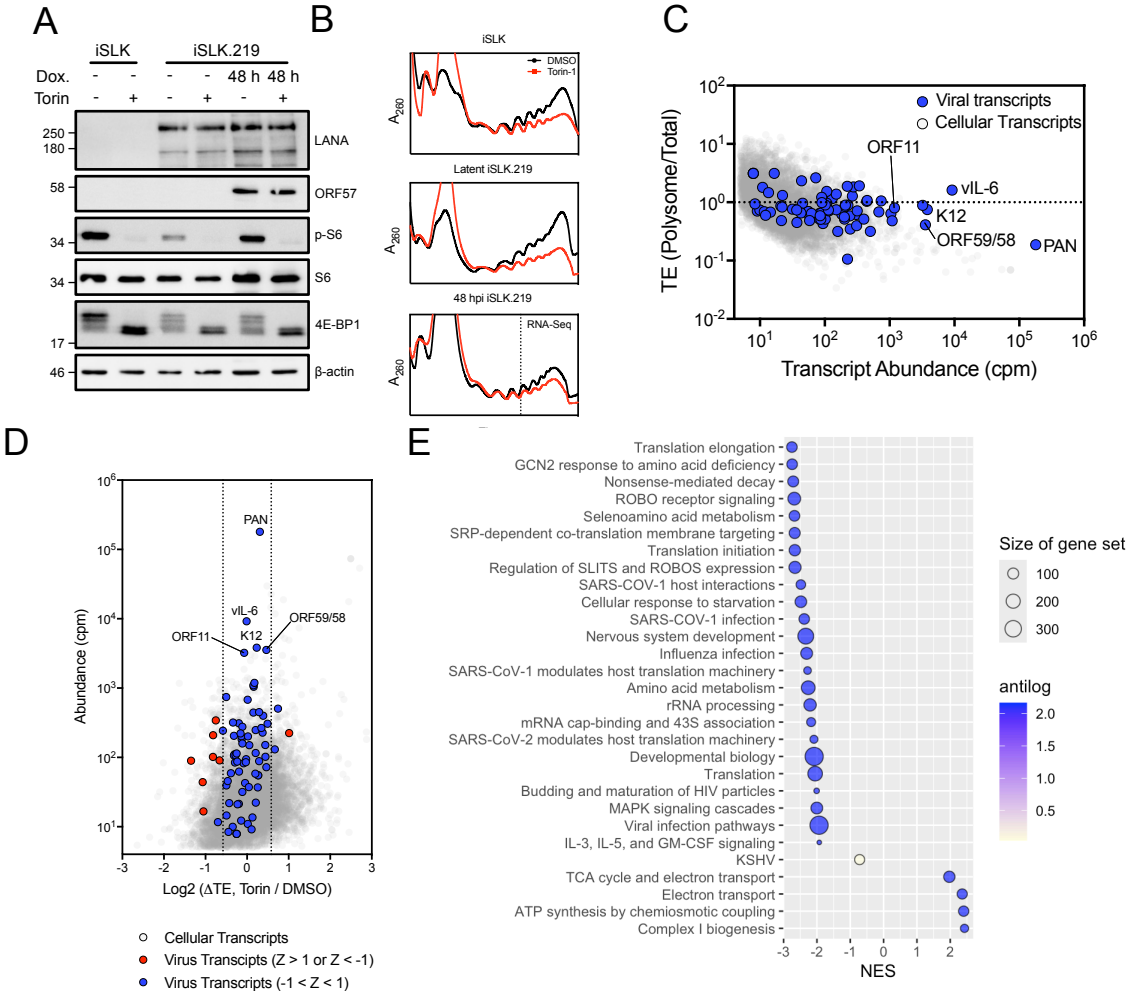

Fig 1. eIF4F disassembly does not affect translational efficiencies of viral mRNAs. (A) Western blots of whole cell lysates of uninfected iSLK, latently infected iSLK.219 and 48hpi iSLK.219 cells treated with Torin or DMSO vehicle control for 2h prior to harvest. **(B)** Polysome profiles of uninfected, latent, or 48 hpi iSLK.219 treated with either Torin or DMSO for 2 h prior to harvest. **(C)** mRNA from translating ribosomes (of DMSO treated cells) was sequenced and aligned to both the human and KSHV genomes. Viral transcripts are depicted in blue on top of the grey background of cellular genes. **(D)** The Δ TE of viral transcripts is depicted in blue or red on a grey background of cellular genes. Viral transcripts beyond one SD of the mean are red, viral transcripts within on SD are depicted in blue. Vertical lines represent a 1.5-fold change in transcript TE. **(E)** Gene set enrichment analysis of transcripts TE < -1.5 Z or TE > 1.5 Z.

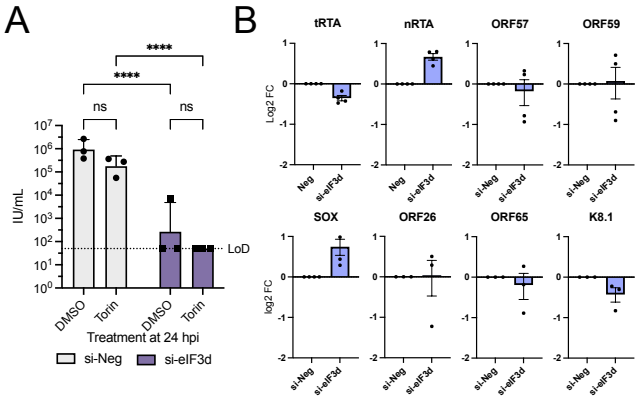

Fig. 2 eIF3D is required for accumulation of KSHV lytic protein products. (A) Titer at 96h from iSLK.219 cells were transfected with siRNA targeting eIF3d or a negative control (n=3; means±SEM; statistical significance was determined by two-way ANOVA). **(B)** RNA was harvested at 72h post-reactivation for RT-qPCR using primers targeting viral gene products as indicated (n=4; means±SEM; statistical significance was determined by two-way ANOVA).

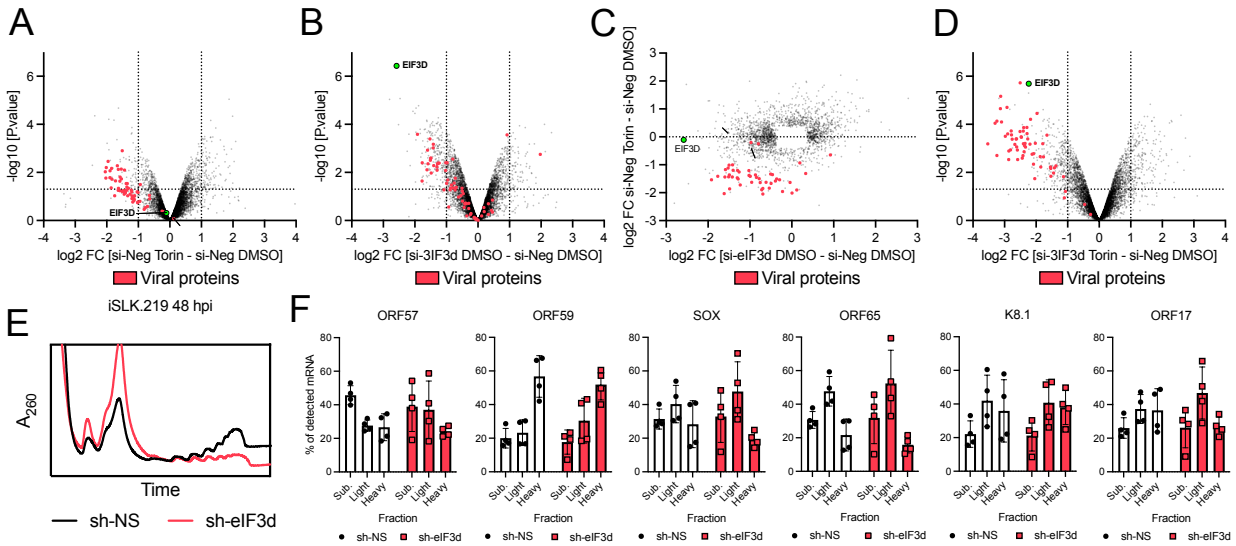

Fig. 3. eIF4F and eIF3d both contribute to protein accumulation during lytic replication. **(A-D)** iSLK.219 cells were transfected with siRNA targeting eIF3d or a negative control and treated with doxycycline the following day. 24h after doxycycline addition the cells were treated with 250 nM Torin of DMSO vehicle control. At 72hpi, total protein was harvested for LC-MS/MS with data-independent acquisition (one m/z window) and label-free quantitation (n=3). Viral proteins are graphed in red and eIF3d is labelled individually. **(A)** si-Neg Torin vs si-Neg DMSO treatment for eIF4F-dependence. **(B)** si-eIF3d vs si-Neg for eIF3d-dependence. **(C)** a comparison of proteins from **(A)** and **(B)** that had a P.Value of < 0.05 in at least one of the samples. **(D)** si-eIF3d treated with Torin vs. si-Neg cells with DMSO treatment for loss of eIF3d and eIF4F. **(E-F)** iSLK.219 cells were transduced with lentiviruses encoding shRNA targeting eIF3d (sh-eIF3d) or a non-targeting (sh-NS) shRNA control. 48h after lytic induction, cells were harvested for polysome analysis. **(E)** Polysome profile of sh-Neg and sh-eIF3d. **(F)** Total RNA was extracted pooled fractions from sub-polysomal, light polysomes, or heavy polysomes and used for RT-qPCR analysis targeting mRNA as indicated. Data is presented as the total amount of detected mRNA detected in each fraction (total mRNA detected = 100%; n=3; means±SEM; statistical significance was determined by two-way ANOVA).

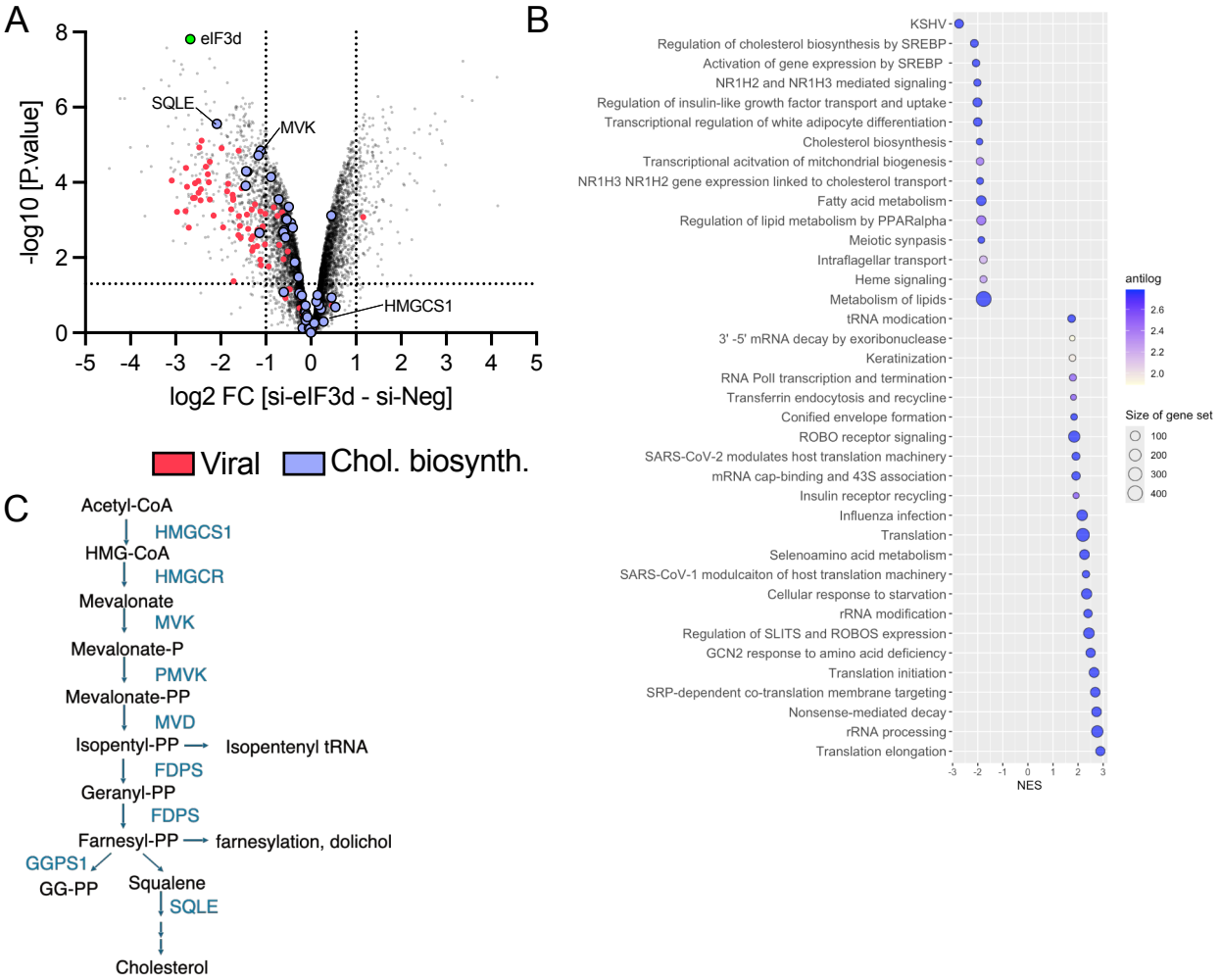

Fig. 4. eIF3d is required for viral protein accumulation and cholesterol biosynthesis during KSHV lytic replication. iSLK.219 cells were transfected with siRNA targeting eIF3d or a negative control and treated with doxycycline the following day. **(A)** Total protein was harvested for LC-MS/MS with data-independent acquisition (three m/z windows) and label-free quantitation (n=3). **(B)** Gene set enrichment analysis with 10% FDR. **(C)** Diagram of the cholesterol biosynthetic pathways. Gene names for Enzymes are in blue.

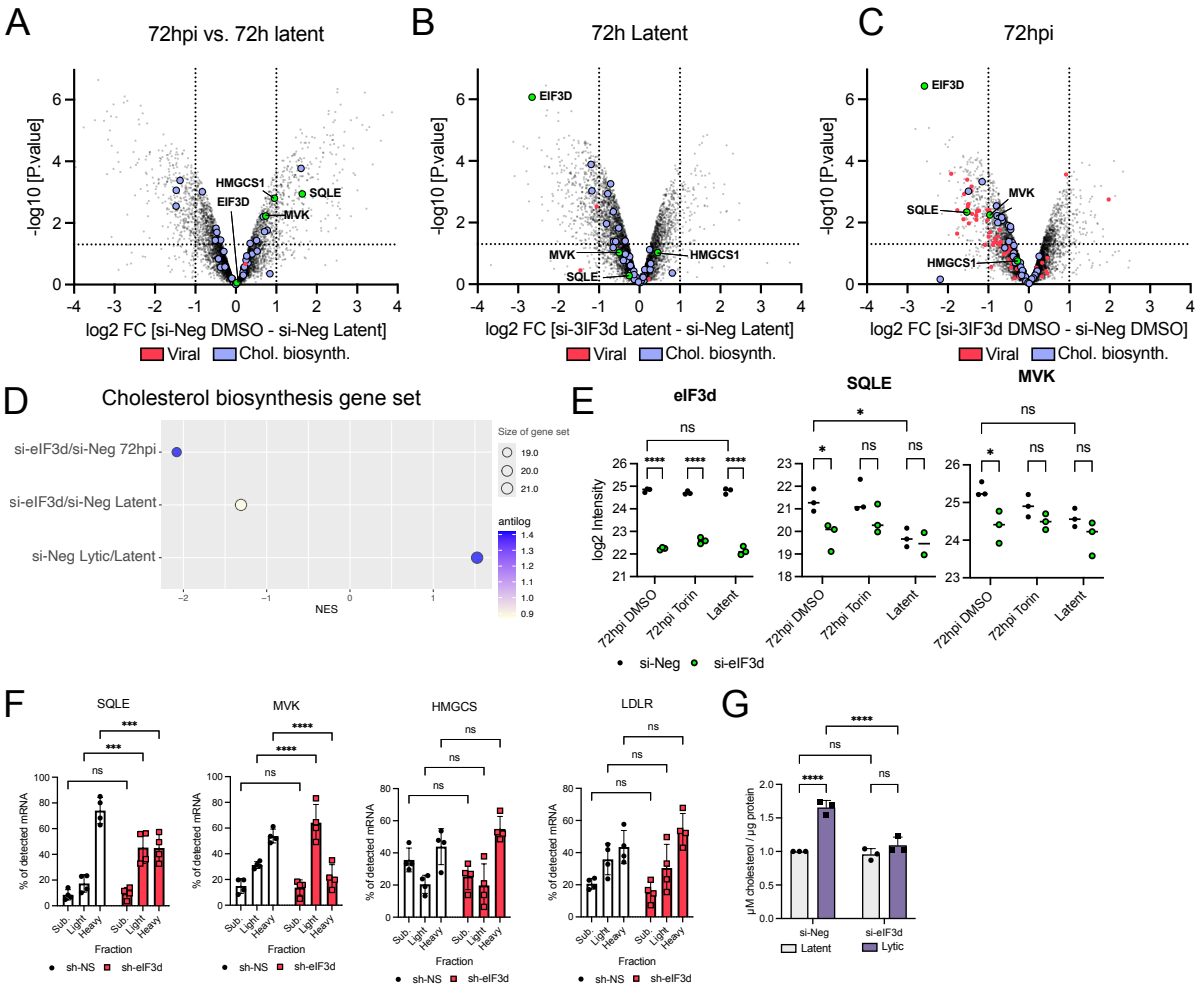

Fig 5. eIF3d is required for efficient translation and accumulation of SQLE and MVK during KSHV lytic replication. (A-C) iSLK.219 cells were transfected with siRNA targeting eIF3d or a negative control and treated with doxycycline the following day. 24h after doxycycline addition the cells were treated with 250 nM Torin of DMSO vehicle control. At 72hpi, total protein was harvested for LC-MS/MS with data-independent acquisition (one m/z window) and label-free quantitation (n=3). Viral proteins are graphed in red; proteins related to cholesterol biosynthesis are in blue; eIF3d, SQLE, and MVK are labelled individually. **(A)** si-Neg Lytic vs. si-Neg Latent for changes associated with lytic replication. **(B)** si-eIF3d vs. si-Neg during latency for eIF3d-dependence in latently infected cells. **(C)** si-eIF3d vs. si-Neg in lytic cells in matched samples of **(A)** and **(B)**. **(D)** Cholesterol biosynthesis GSEA for **(A-C)** **(E)** log2 transformed intensity value for eIF3d, SQLE, and MVK as measured for values represented in **(A-C)**. **(F)** Polysome analysis of cholesterol biosynthesis genes as in **Fig. 3E-F.** (total mRNA detected = 100%; n=3; means±SEM; statistical significance was determined by two-way ANOVA). **(G)** Quantification of cholesterol abundance by luciferase-based reporter assay normalized to total protein quantity (n=3±SEM; statistical significance was determined by two-way ANOVA)

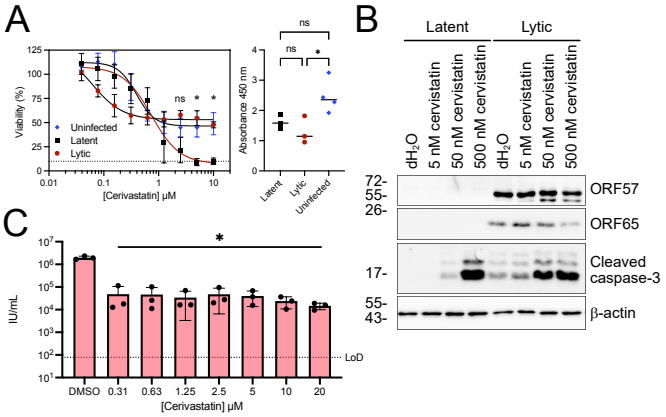

Fig. 6. (A) Uninfected iSLK, latently infected, or lytically replicating iSLK.219 cells treated with varying concentrations of HMGCR inhibitor cerivastatin. Viability was determined at 48h using colourimetric CCK-8 assay (n=3-4; means±SEM; statistical significance was determined by one-way ANOVA). **(B)** Western blot of latent or lytic iSLK.219 at 48hpi treated with cerivastatin for 48h. Lysates were probed as indicated. **(C)** Virus titer at 96hpi from iSLK.219 cells treated with varying concentrations of cerivastatin (n=3-4; means±SEM; statistical significance was determined by two-way ANOVA).